Global Particle Simulation Study of Substorm Onset and Particle Acceleration

Ken Nishikawa (*Rutgers University*)

Shin Ohtani (*APL/JHU*)

Dong-Sheng Cai (*University of Tsukuba*)

Bertrand Lembège (*CETP/UVSQ/IPSL*)

EGS meeting, April 21 - 26, 2002

Abstract

We report the spatial and temporal development of **Bursty Bulk Flows (BBFs)** created by the **reconnection** as well as **current disruptions (CDs)** in the near-Earth tail using our **3-D global EM particle simulation with a southward turning IMF** in the context of the substorm onset. Recently, observations show that **BBFs** are often accompanied by current disruptions for **triggering substorms**. We have examined the dynamics of BBFs and CDs in order to understand the timing and triggering mechanism of substorms. As the solar wind with the southward IMF advances over the Earth, the near-Earth tail thins and the sheet current intensifies. Before the peak of the current density becomes maximum, the local **reconnection** takes place locally, which ejects particles from the reconnection region. Because of the **earthward flows** the peak of the current density moves toward the Earth. The characteristics of the earthward flows depend on the ions and electrons**.**

Electrons flow back into the inflow region (the center of reconnection region), which provides current closure. Therefore the structure of electron flows near the reconnection region is rather complicated. In contrast, the ion earthward flows are generated far from the reconnection region. These earthward flows pile up near the Earth. The ions mainly drift toward the duskside. The electrons are diverted toward the duskside. **Due to the pile-up, dawnward current is generated near the Earth.** This dawnward current dissipates rapidly with the sheet current because of the opposite current direction, which coincides with the dipolarization in the near-Earth tail. At this time the **wedge current may be created in our simulation model.** This simulation study shows the sequence of the substorm dynamics in thenear-Earth tail, which is similar to the features obtained by the multisatellite observations. The identification of the timing and mechanism of triggering substorm onset requires further studies in conjunction with observations.

Motivations

- Take advantage of modern supercomputers using parallel processing (HPF) on ORIGIN2000
- Kinetic processes reveal essential physics involved in substorms and storms
- Investigate energetic particle injections into inner magnetosphere and ionosphere originated from the solar wind particles
- Contribute to new NASA missions such as Cluster II, Magnetospheric Multiscale Mission and Magnetospheric Constellation that provide data with microscopic processes (velocity distributions) with future significant improvements in simulation and physical parameters
- 3-D Electromagnetic Particle Model (EMPM) for Space Weather Program is a challenging project, however it is necessary for predicting high energy particle injections

Objectives

- What is the time sequence of tail dynamics with southward turning IMF?
- When does the reconnection take place?
- How are earthward flows (BBFs) generated?
- What is the relationship among reconnection, BBFs, flow braking, and CD?
- When and how does the dipolarization occur?
- What is the main mechanism of substorm triggering?
- How does the IMF B_y component affect these processes?

Summary of simulations

Solar wind with southward IMF

↓

Sheet current becomes maximum

(Local reconnections occur)

↓

***Full* Reconnection takes place**

↓ ↓

Peak of sheet current moves Earthward | **Earthward flows are generated**

↓ ↓

Current disruption | **Flows brake**

↓ ↓

Dipolarization | **Dawnward current**

↓ ⇩ ↓

Wedge Current is generated?

SIMULATION RESULTS

Please refer to [*Nishikawa* 1997, 1998a, b; *Nishikawa and Ohtani*, 2000a, b; *Nishikawa*, 2001] for the initial and boundary conditions and parameters used in our simulations.

The simulation grid **D »1 RE**. The **time step D t » 10 seconds**
1152: 00.00UT; 1216: 00.10UT; 1280: 00.20UT;
1344: 00.30UT; 1408: 00.40UT; 1472: 00.50UT

Figure 1: shows the magnetic field lines in the noon-midnight meridian plane (GSM). **Figure 1c displays the thinned magnetotail and other diagnosis shows the local reconnection**. Figure 1d shows **magnetic reconnection occurring at 0.20UT (1280),** near $x = 85\Delta$ (≈ -15 RE).

Figure 2 shows the **averaged current density** is plotted along the *x* direction at [*Nishikawa and Ohtani*, 2000a]. The **dawnward current is generated at 0.10UT (1216), and it increases at 0.20UT (1280). It disappears at 0.30UT (1344) with the dipolarization.** Because of the ejection by the reconnection, particles are injected into the magnetosphere, and **the peaks of the current density also move toward the Earth as seen at 0.10UT (1216), 0.20UT (1280), and 0.30UT (1344**).

Magnetic field lines in 2-D (noon-midnight)

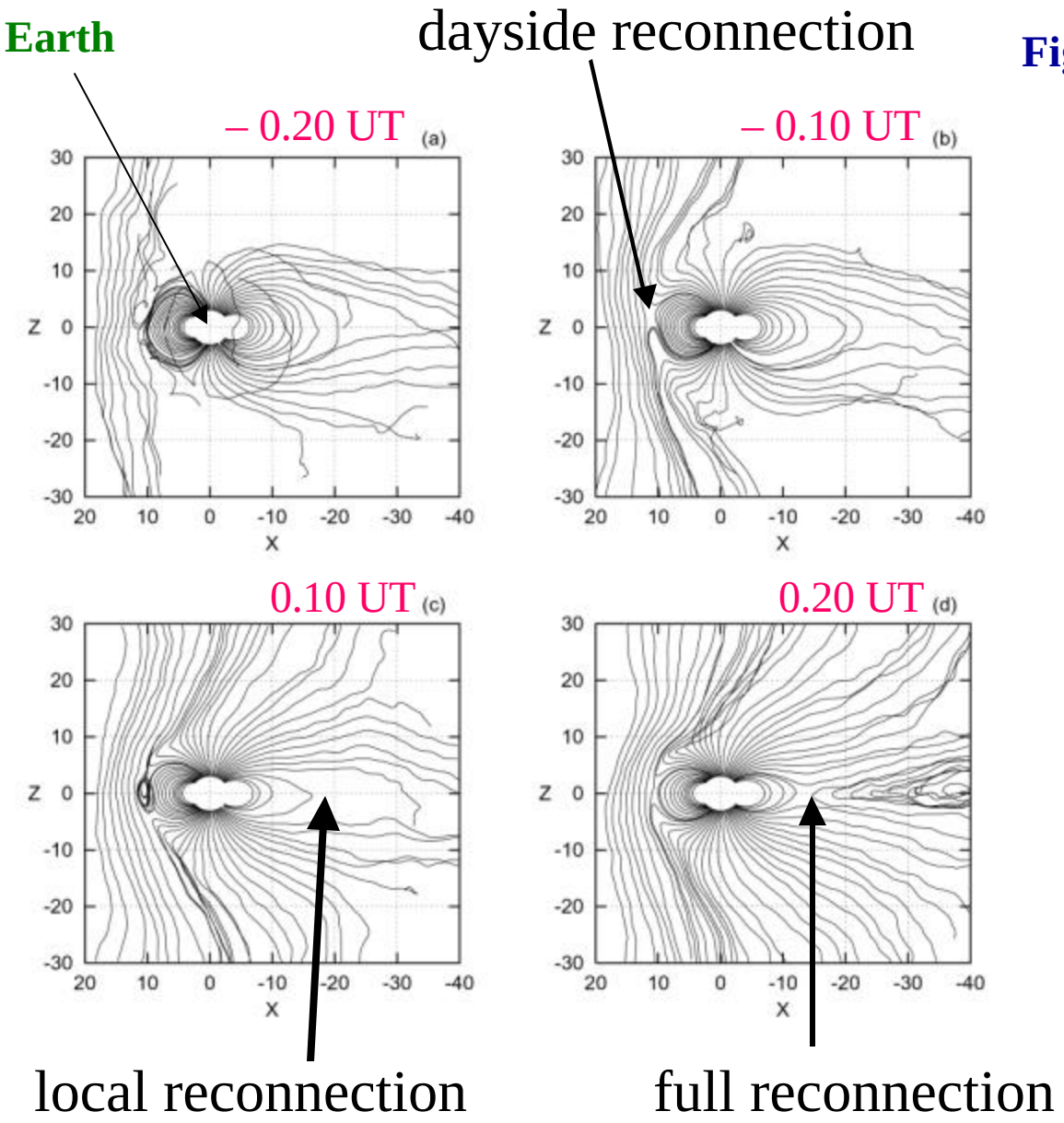

Figure 1 shows the magnetic field lines in the noon-midnight meridian plane (GSM) containing the dipole center at step (a) – 0.20 UT (1024), (b) – 0.10 UT (1088), (c) 0.10 UT (1216), and (d) 0.20 UT (1280). The magnetic field lines are traced from near the Earth ($r = 3\Delta$, ($\approx 3R_E$)) and subsolar line in the dayside and the magnetotail. Some magnetic field lines are moved dawnward or duskward. The tracing was terminated due to the preset number of points or the minimum strength of total magnetic field.

Averaged current density J_y (× 10) along the subsolar line

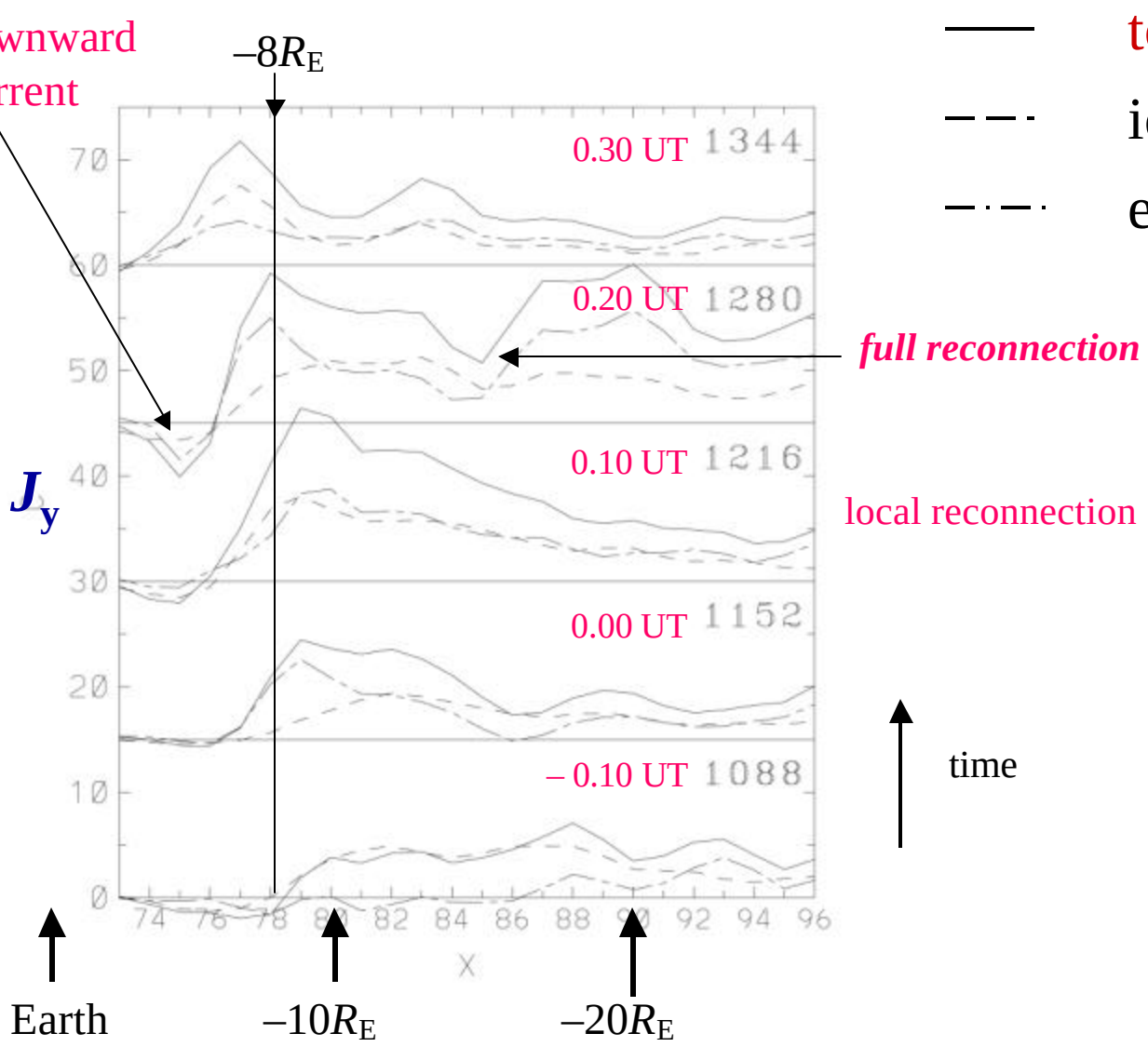

Figure 2 shows the **averaged current density** J_y in the noon-midnight meridian cross section at time – 0.10 UT (1088), 0.00 UT (1152), 0.10 UT (1216), 0.20 UT (1280), and 0.30 UT (1344) [*Nishikawa and Ohtani*, 2000a].

The gradient of current sheet becomes very steep at 0.20UT (1280). It is proposed that **the wedge current is generated by the dawnward inertia current** [e.g., *Haerendel*, 1992; *Shiokawa et al*., 1997, 1998a]. **Flux (left column) and velocity (right column) in the plasma sheet** ($45 < z/\Delta < 51$) and the north and south lobes (outside the plasma sheet) are plotted at 0.20UT (1280) after the reconnection takes place (***flux*** **= S*v*$_x$(i)** and ***v*** **= S*v*$_x$(i)/S i)**

Figure 3 shows the ion flux and velocity in the dusk-dawn cross section plane at $x = -8\ R_E$ (a and b), $-10\ R_E$ (c and d), $-12\ R_E$ (e and f), $-14\ R_E$ (g, and h). The **earthward ion flux (blues)** increases near the Earth ($x = -8R_E$ (Fig. 3a). The earthward high velocity (blues) is seen in the **duskside** as shown in Fig. 3b.

Figure 4 shows electron flux and velocity at the same time. In contrast to the ion earthward fluxes, **earthward electron fluxes are found near the reconnection region** ($x \approx -15\ R_E$) as shown in Fig. 4g. It should be noted that **the tailward flux is mixed with the earthward flux, which indicates the generation of current closure near the null points (the 3-dimensional reconnection)** [*Cai et al., 2001*] (more complicated than the X point in the 2-dimensional simulation) [*Sonnerup*, 1979; *Terasawa*, 1983].

ion flux 0.20 UT velocity in the x – z plane **viewed from the tail**

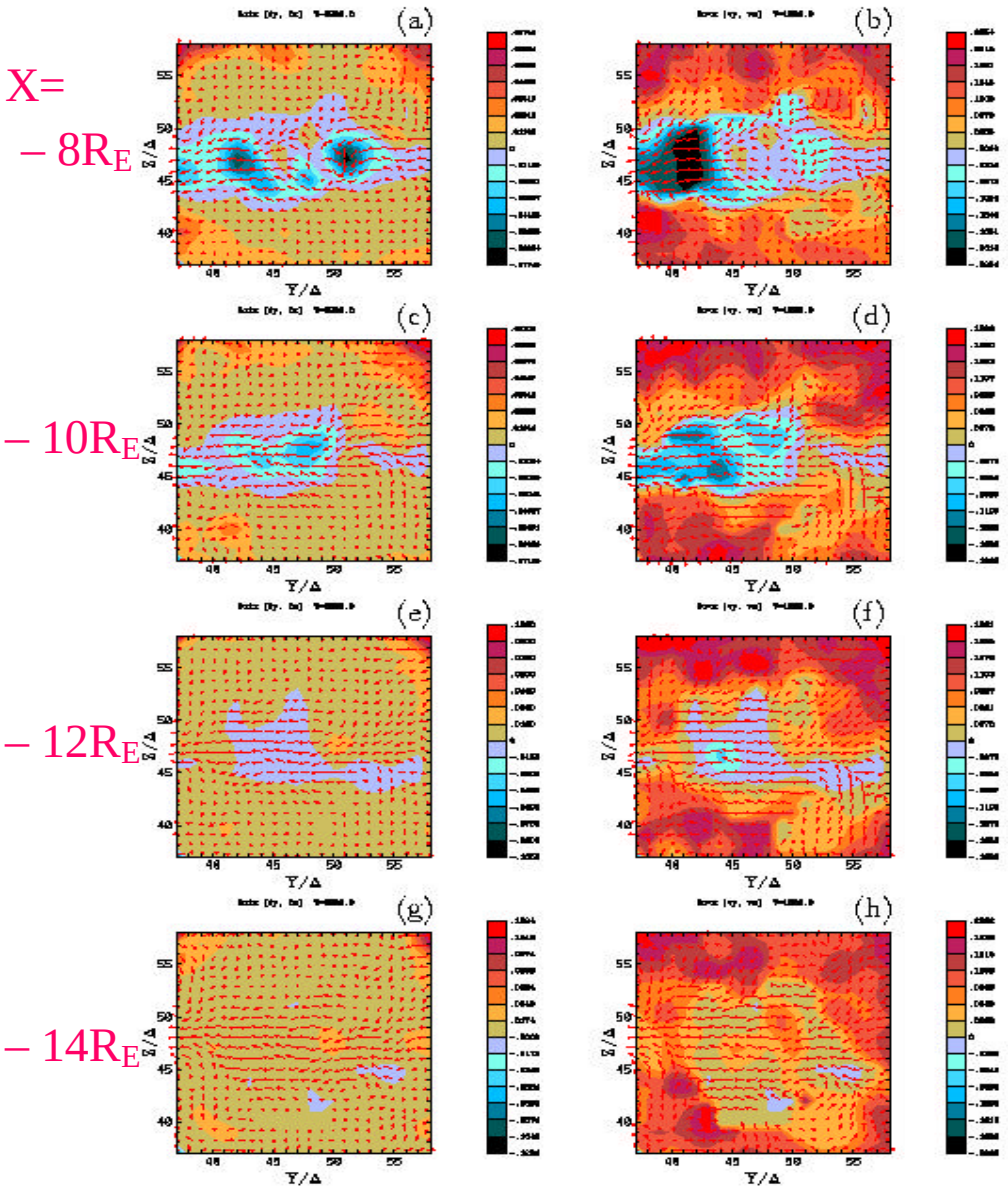

blues: earthward

reds: tailward

Figure 3 shows the ion flux (a, c, e, and g) and velocity (b, d, f, and h) in the dusk-dawn cross section plane at $x = -8\ R_E$ (a and b), $-10\ R_E$ (c and d), $-12\ R_E$ (e and f), $-14\ R_E$ (g and h) at time 0.20 UT (1280).

arrows: (V_y, V_z)

electron flux 0.20 UT velocity in the x – z plane **viewed from the tail**

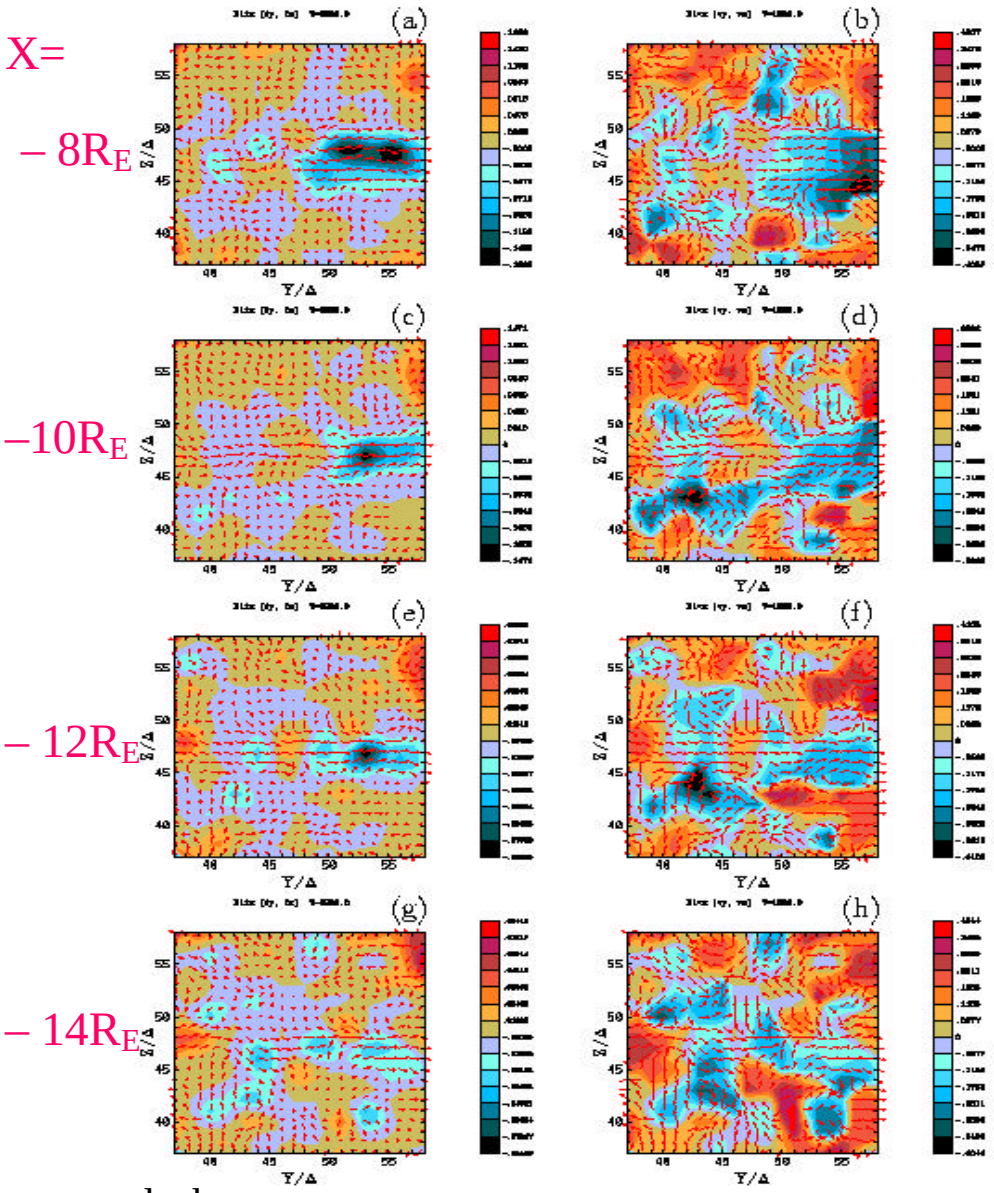

blues: earthward

reds: tailward

Figure 4 shows the electron flux (a, c, e, and g) and velocity (b, d, f, and h) in the dusk-dawn cross section plane at x = –8 R_E (a and b), –10 R_E (c and d), –12 R_E (e and f), –14 R_E (g and h) at time 0.20 UT (1280).

arrows: (V_y, V_z)

High earthward electron flux is confined to the plasma sheet, however, earthward high velocity electrons are found in the outside of the central plasma sheet, since electrons are accelerated along the magnetic separatrices (Fig. 4).
Electrons are diverted mainly toward the dawn as expected. The highest earthward electron velocity reaches about 4 times the electron thermal velocity in the solar wind (**about 150% of the solar wind velocity**).

Figure 5 shows the time evolution of ion and electron velocity in the dusk-dawn cross section plane at $x = -10R_E$. **The erathward high ion velocity (blues) in the dawnside at 0.10UT (1216) (Fig. 5a) decreases at later time** (Fig. 5c and 5e). In contrast, **earthward high velocity electrons remain almost the same at later time** as shown in Fig. 5b, 5d, and 5f.

Figure 6 shows the ion and electron velocities (the v_x: color, $v_{x,y}$: arrows) in the equatorial plane. **Ions are mainly diverted toward the dusk** (Fig. 6a, 6c, and 6e), and **electrons are diverted toward the dawn** (Fig. 6b, 6d, and 6f). As shown in electron velocity structures (in the right column), **near the Earth (within $10R_E$) the electron velocities look irregular because of the turbulence, which supports an evidence of occurrence of CCI** (see also Figs. 5b, 5d, 5f, 6c, and 6d).

ion velocity electron dusk-dawn plane at x = –10 R_E

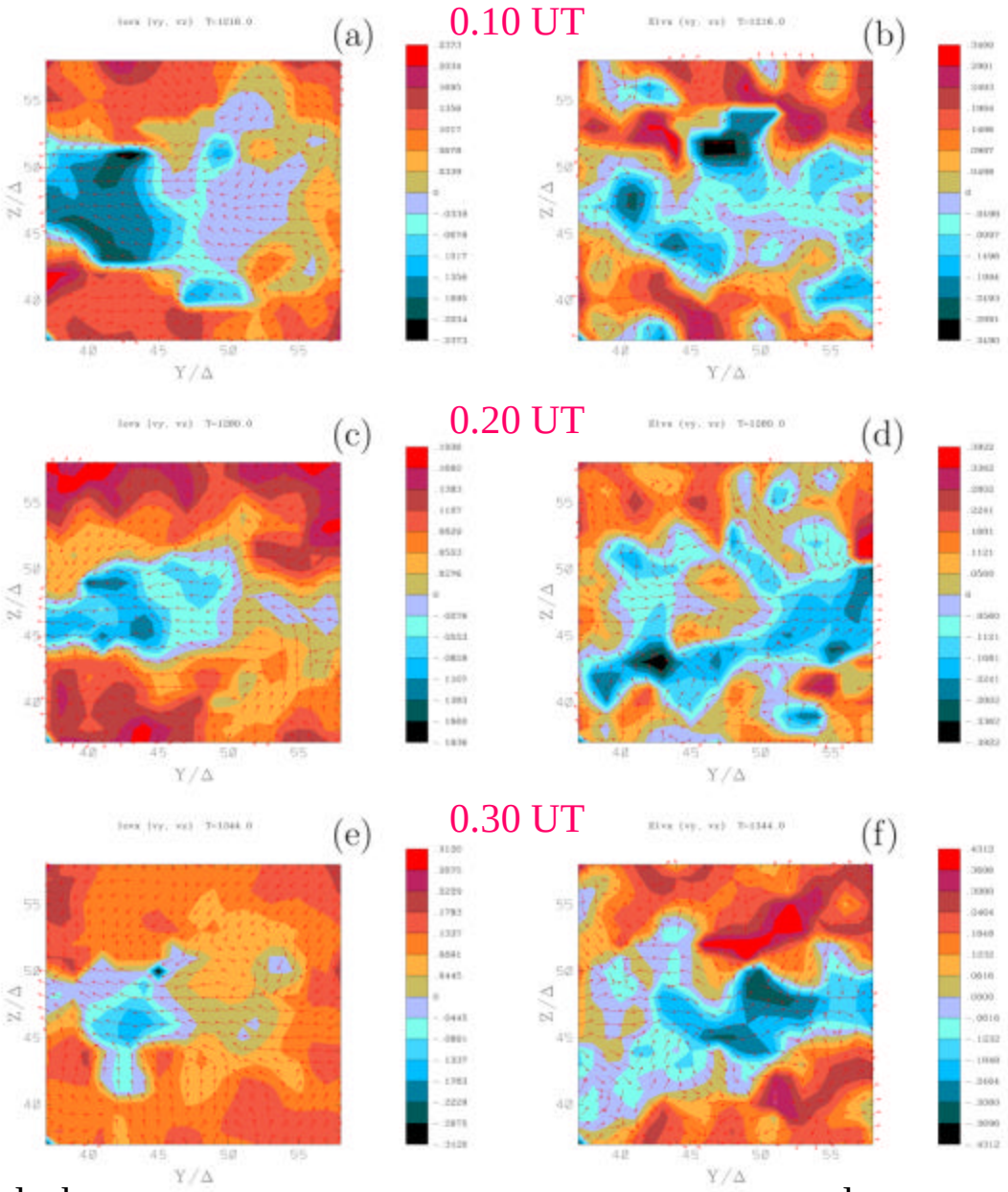

viewed from tail

blues: earthward

reds: tailward

arrows: (V_y, V_z)

Figure 5 shows evolution of ion (a, c, and e) and electron (b, d, and f) velocities on the dusk-dawn cross section plane at x = 80Δ at time (a and b) 0.10 UT (1216), (c and d) 0.20 UT (1280), and (e and f) 0.30 UT (1344). The arrows show the ion (a, c, and e) and electron (b, d, and f) velocities on the plane (rescaled to show small values).

ion electron velocity at the equatorial plane

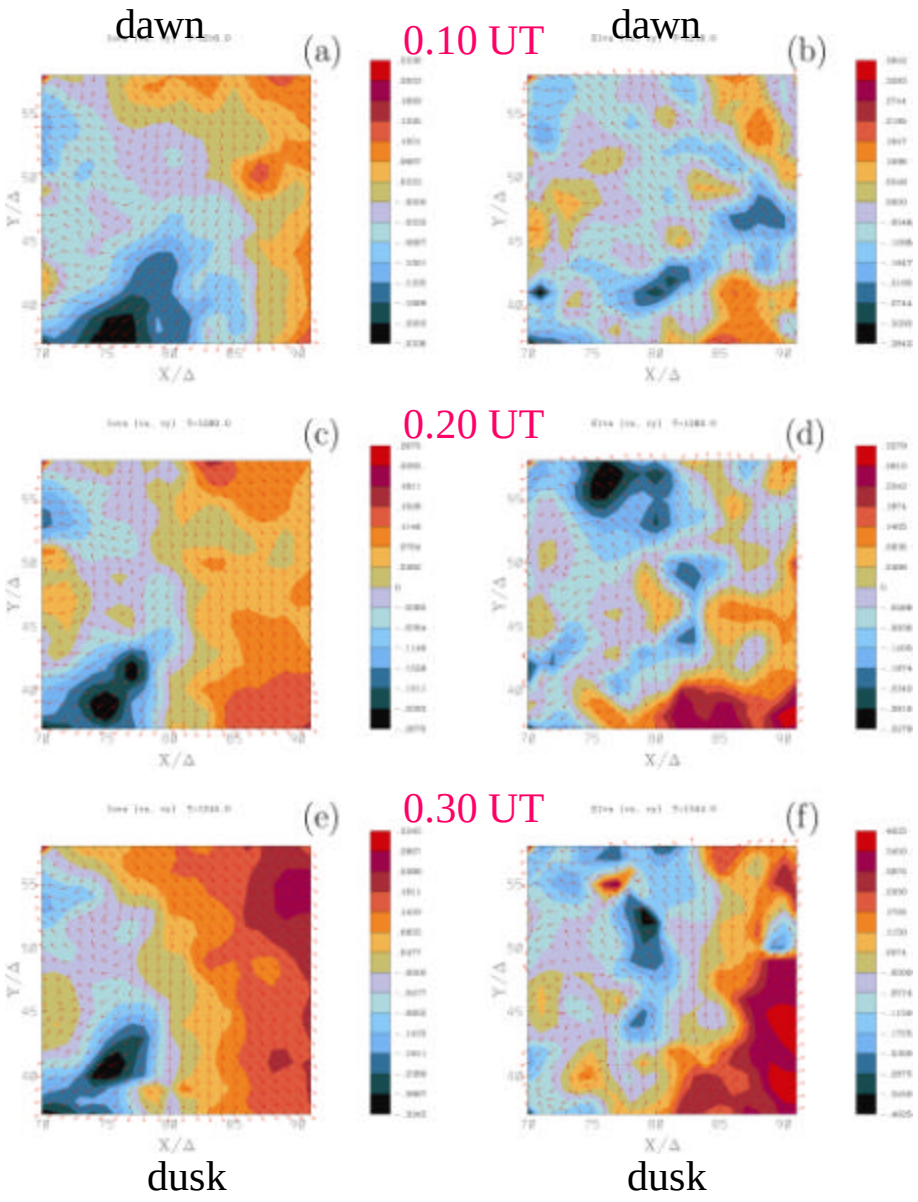

blues: earthward

reds: tailward

arrows: (V_x, V_y)

Figure 6 shows evolution of ion (a, c, and e) and electron (b, d, and f) velocities in the equatorial plane at z = 48Δ at time (a and b) 0.10 UT (1216), (c and d) 0.20 UT (1280), and (e and f) 0.30 UT (1344). The arrows show the ion (a, c, and e) and electron (b, d, and f) velocities on the plane (rescaled to show small values).

Earth

Figure 7 shows total magnetic field strength (log(|B|(x,y,z)|) at *y = 47D*) **in the noon-midnight cross-section (*x* - *z*) plane** in the near-Earth magnetotail. At 0.00UT (1152) (Fig. 7a) the arrows show an ordinary stretched dipole magnetic field. The further stretching of the magnetic field is found in the weakening normal component (B_z) (still positive) in the central sheet (Fig. 7b). At 0.20UT (1280) **the X point is created**, which shows **the occurrence of reconnection around x = 85D (» -15R_E)** as shown in Fig. 7c. The boundary line at value –0.4 moves toward the tail at 0.20UT (1280). This comes from the magnetic transfer by the reconnection. Further dipolarization takes place in the near-Earth magnetotail as shown in Fig. 7d. As shown in Figure 2, the dipolarization coincides with the current decrease at time step 1344.

Figure 8 shows the differences of the B_z in the equatorial plane from that at 0.00UT (1152) when the southward IMF effects are not visible yet (Fig. 8a). **At 0.10UT (1216) the B_z decreases near the Earth shown by blues (Fig. 8b).** As shown in Fig. 8c **the B_z decreases in the entire region. At 0.30UT (1344) the B_z increases locally near the Earth shown by reds, which shows the dipolarization.** After the reconnection, the dipolarization takes place near the Earth at 0.30UT(1344) as shown in Fig. 8d.

Diploarization seen in the noon-midnight meridian plane

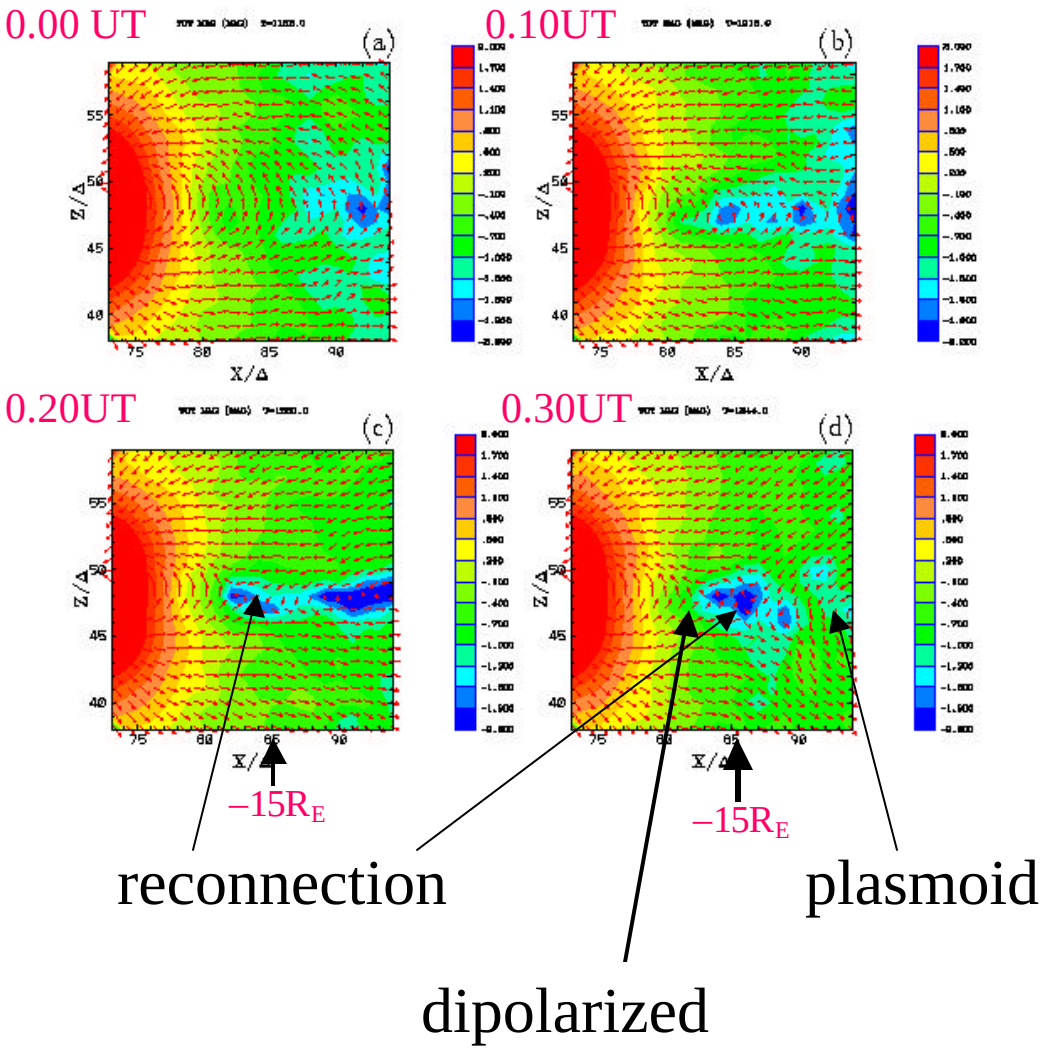

Figure 7 shows the ***total magnetic field*** strength in the noon-midnight meridian cross section ($x - z$) plane in the near-Earth magnetotail at time (a) 0.00 UT (1152), (b) 0.10 UT (1216), (c) 0.20 UT (1280), and (d) 0.30 UT (1344). The arrows show the magnetic field.

Earth

Diploarization seen in the equatorial plane

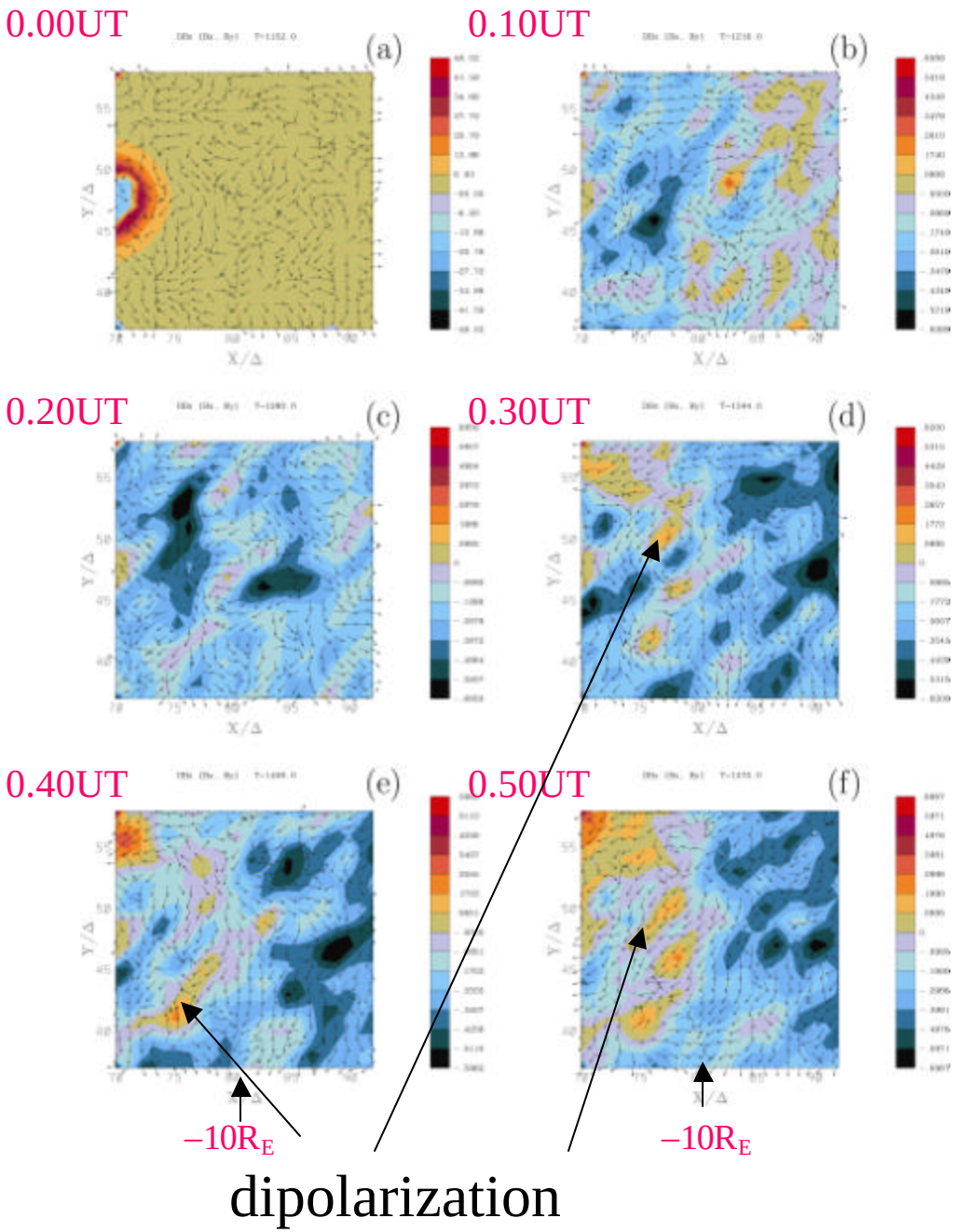

reds: increased

blues: decreased

Figure 8 shows time evolution of the ***B_z magnetic field component*** subtracted by the value at time 0.00 UT (1152) (a) in the equatorial (x - y) plane near the Earth magnetosphere at time (b) 0.10 UT (1216), (c) 0.20 UT (1280), (d) 0.30 UT (1344), (e) 0.40 UT (1408), and (f) 0.50 UT (1472). The arrows show the magnetic field in the equatorial plane.

Earth

arrows (B_x, B_y)

Field-aligned currents at the north pole at $r = 5\ R_E$

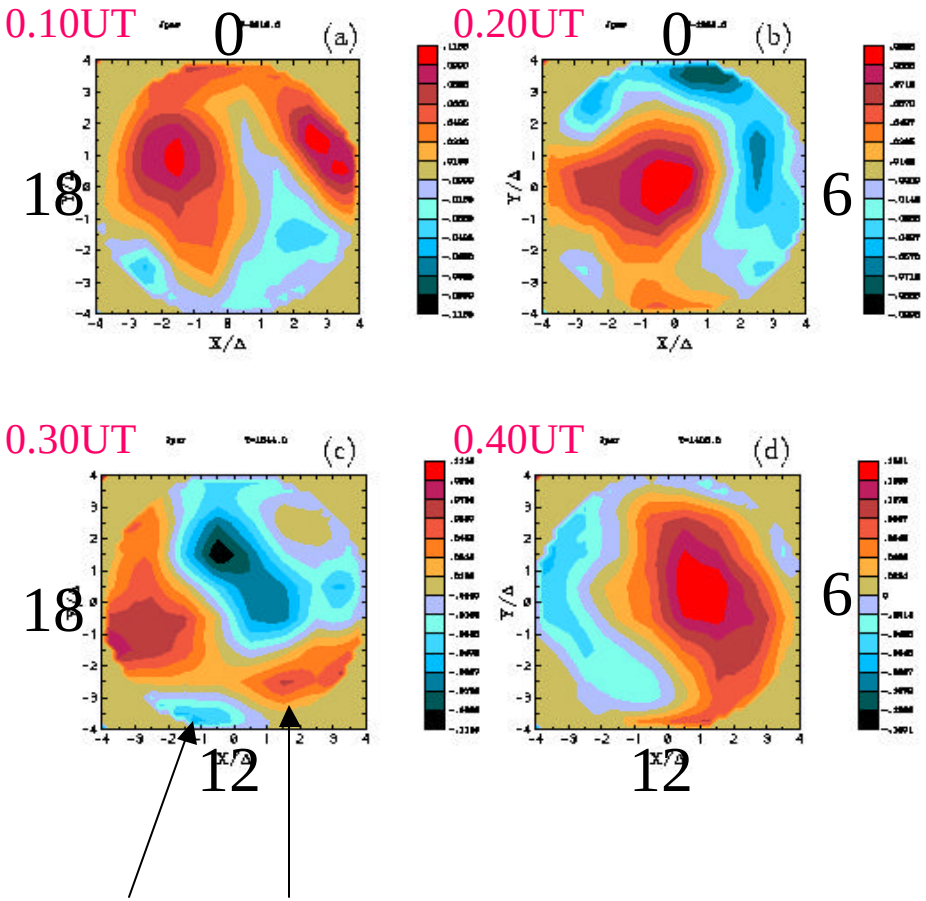

latitudes: 37°- 90°

Figure 9 shows time evolution of the field aligned current at $r = 5\Delta$ ($\approx 5\ R_E$)) around the north pole (90° -- 36.9°) (projected on the equatorial plane and viewed from the pole). (a) 0.10 UT (1216), (b) 0.20 UT (1280), (c) 0.30 UT (1344), and (d) 0.40 UT (1408). The inward and outward currents are shown by blues and reds, respectively.

blues: inward

reds: outward

needs further improvements!

DISCUSSION

The evolution of near-Earth tail with a southward turning IMF is studied in order to address **the cause-and-effect relationship between the reconnection, BBFs, flow braking, and current disruption.** Our 3-D global EM particle simulation results show that the cross-field current is enhanced at the substorm growth phase with a southward IMF. The duskward electric field accompanied by the southward IMF begins to enhance the current sheet in the near-Earth magnetotail. The current sheet is thinned, and at the same time the local reconnection takes place [*Cai and Nishikawa*, 1999]. **Later the (full) reconnection takes place and ejects particles, which Generates (high-velocity) ion and electron flows in the near-Earth tail** as shown in Figures 1 - 8. The dawnward current is generated by the braking of earthward flows. **Due to the dawnward current the gradient of current density near the Earth (-5 R_E > x > -8 R_E) becomes very steep at 0.20UT (1280).**

On the basis of these simulation results we infer that the current disruption plays a role in triggering substorm onset in assistance with the flow braking of earthward flows generated by the reconnection.

The field-aligned current at r = 5R_E on the north pole is examined in order to check the validity of the present simplest ionospheric response in which particles are reflected by the mirror force in the cusps. (The parallel current is calculated by $J_{\|}$ = **J•B/B**.) This ionospheric model includes the **ambipolar field** and **effects of gyromotion** in the dipole magnetic field near the Earth (grad-B/curvature currents).

Figure 9 shows **the time evolution of field-aligned currents (FACs) which are projected on the equatorial plane.** The **inward** (into the ionosphere) current is shown by **blues** and **outward** (tailward) currents are plotted by **reds**. The upper side is faced toward the Sun and the right side is faced toward the dawn. The latitude ranges from 90° to 37°. As expected at least a pair of inward and outward currents is found. The intensity of current is not changed except at 0.40UT (1408). At 0.30UT (1344) (Figure 9c) two pairs of currents are found with the dipolarization (see Fig. 7c) and this current pattern is consistent with a schematic diagram of field-aligned current shown in Plate 4 in [*Birn et al.*, 1999]. **The pair with a stronger current near the pole may correspond to the region I current and another pair with a weaker current in the nightside may correspond to the region II current. In order to examine the FACs obtained by our simulations, the question how FACs are closed at the inner boundary (at the ionosphere (r » 2 R_E)) needs to be answered.** We also need to improve the ionospheric model in our simulations including the ionospheric dynamics such as ionospheric outflows.

Summary

- Simulation with a southward IMF shows the sequence of substorm processes, which is similar to the observations
- Due to the local reconnection and the convection electric field ($E \approx -V_{sol} \times B_{IMF}$), earthward flows enhance the sheet current at the near the Earth, which leads to current disruption
- A wedge current is created due the synergetic effects of reconnection, CD, and dipolarization
- In order to investigate the substorm and storm dynamics a new simulations with better resolutions and more realistic ionospheric models
- Global particle simulation will be a vital model for Space Weather Program and future investigations with multi-satellite missions such as MMS and MC DRACO

Future Plans

- Run simulations with better resolutions using **HPF Tristan** code on **ORIGIN2000**
- Simulations related to magnetic storms including **magnetic plasma clouds**
- Using satellite date for initial solar wind conditions perform **case studies** to compare with observations
- **Improve 3-D displays** in order to understand physics involved with **AVS**
- Implement **a better ionospheric model** **including ionospheric outflows**
- Investigate **high energy particle injections** into the ionosphere
- **Predict energetic particle injection** in conjunction with magnetic storms with typical solar wind parameters

Evolution of thin sheet current with a southward IMF by a 3-D EM particle code

K.-I. Nishikawa and S. Ohtani, (JGR, 105, 13,017, 2000)

Global Particle Simulation Study of Substorm Onset and Particle Acceleration

K. I. Nishikawa, (Space Science Review, 95, 361, 2001)

available at http://www.physics.rutgers.edu/~kenichi

Name Address
